Plasma parameters of pulsed-dc discharges in methane used to deposit diamondlike carbon films

C. Corbella,[a] M. Rubio-Roy, E. Bertran, and J. L. Andújar
FEMAN Group, IN²UB, Departament de Física Aplicada i Òptica, Universitat de Barcelona, c/Martí i Franquès 1, E-08028 Barcelona, Spain

(Received 4 February 2009; accepted 24 June 2009; published online 5 August 2009)

Here we approximate the plasma kinetics responsible for diamondlike carbon (DLC) depositions that result from pulsed-dc discharges. The DLC films were deposited at room temperature by plasma-enhanced chemical vapor deposition (PECVD) in a methane (CH_4) atmosphere at 10 Pa. We compared the plasma characteristics of asymmetric bipolar pulsed-dc discharges at 100 kHz to those produced by a radio frequency (rf) source. The electrical discharges were monitored by a computer-controlled Langmuir probe operating in time-resolved mode. The acquisition system provided the intensity-voltage (*I-V*) characteristics with a time resolution of 1 μs. This facilitated the discussion of the variation in plasma parameters within a pulse cycle as a function of the pulse waveform and the peak voltage. The electron distribution was clearly divided into high- and low-energy Maxwellian populations of electrons (a bi-Maxwellian population) at the beginning of the negative voltage region of the pulse. We ascribe this to intense stochastic heating due to the rapid advancing of the sheath edge. The hot population had an electron temperature T_e^{hot} of over 10 eV and an initial low density n_e^{hot} which decreased to zero. Cold electrons of temperature $T_e^{\mathrm{cold}} \sim 1$ eV represented the majority of each discharge. The density of cold electrons n_e^{cold} showed a monotonic increase over time within the negative pulse, peaking at almost 7×10^{10} cm^{-3}, corresponding to the cooling of the hot electrons. The plasma potential V_p of ~ 30 V underwent a smooth increase during the pulse and fell at the end of the negative region. Different rates of CH_4 conversion were calculated from the DLC deposition rate. These were explained in terms of the specific activation energy E_a and the conversion factor x_{dep} associated with the plasma processes. The work deepens our understanding of the advantages of using pulsed power supplies for the PECVD of hard metallic and protective coatings for industrial applications (optics, biomedicine, and electronics). © *2009 American Institute of Physics*. [DOI: 10.1063/1.3183945]

I. INTRODUCTION

Plasma technology is fundamental for the deposition and processing of hard coatings.[1,2] Nowadays, magnetron sputtering and PECVD are the most popular industrial plasma coating methods.[3,4] Pulsed-dc technology has led to the design of cost-effective deposition systems and to improved film properties, compared to previous rf systems.[5,6] Besides reducing powder formation and allowing more precise control of the generation of reactive species, the use of pulsed-dc power has led to the possibility of large-scale plasma deposition processes. This is a very important issue for industry, as it offers the possibility of coating large areas and increasing the deposition throughput,[7,8] especially in the production of polymers,[9,10] flat panel displays,[11,12] and both functional and protective coatings.[13–17] Moreover, this technology has permitted the development of more sophisticated equipment with additional ionization sources[18,19] and has led to the production of innovative materials. Specifically, the use of an asymmetric bipolar pulsed-dc power source operating between 50 and 350 kHz is advantageous for the effective PECVD of DLC films. DLC contains an amorphous network of sp^2- and sp^3-bonded carbon atoms, which confers mechanical and tribological properties similar to those of diamond, such as hardness, resistance to wear, and a low friction coefficient.[20–23]

Thanks to pulsed power supplies, the PECVD of DLC films has achieved higher growth rates and lower stress levels.[24] The waveform of the signal driven to the cathode and also the power input into the glow discharge *W* have a strong influence on the properties of the growing film. The energy of the ions impinging onto the DLC film has a decisive influence on its structure and hydrogen content.[21,25] Whereas in the case of a rf power source the maximal ion energy is limited by the self-bias potential U_{sb}, pulsed-dc plasmas provide local peak voltages with amplitudes so large that they result in a much more intense and energetic ion bombardment. The use of pulses has also beneficial effects when growing DLC and metal-containing DLC films by pulsed-dc reactive magnetron sputtering.[26,27]

Used in parallel with film deposition, plasma diagnostics ensure process control and reproducibility of the process. Optical emission spectroscopy (OES),[28,29] quadrupole mass spectrometry (QMS),[30,31] and diagnostics by means of a retarding field energy analyzer (RFEA)[32] and a Langmuir probe[33–35] are the most common plasma characterization techniques. The last of these provides reliable monitoring of plasma parameters by means of recording *I-V* characteristics

[a]Author to whom correspondence should be addressed. Electronic mail: corbella@ub.edu.

from an electrostatic tip in the glow discharge. However, the evaluation of these parameters in nonstationary processes requires the acquisition of *I-V* curves by Langmuir probes configured in a time-resolved mode. Much progress has been reported concerning time-resolved tracking of electron temperature, plasma density, and potentials in pulsed plasmas.[36–38] Such analysis increases our understanding of the plasma kinetics in discharges with time-varying patterns and involving a huge variety of gases. Hydrocarbons are the main precursors for the synthesis of DLC films: propane (C_3H_8),[39] benzene (C_6H_6),[40] acetylene (C_2H_2), and CH_4 are of particular importance.[21,41–43] Although C_2H_2 produces harder films and faster deposition, CH_4 is commonly used to coat electronic devices and is less harmful.[21] The precursor can be mixed with other gases such as argon (Ar) and hydrogen (H_2) in order to modify the plasma chemistry and the surface morphology.

In this paper, the deposition of DLC in a pure CH_4 atmosphere at 10 Pa was performed by 100 kHz pulsed-dc PECVD and monitored by means of a fast Langmuir probe. The plasma parameters were calculated at 1 μs interval, and their evolution within the pulse cycle and against *W* is discussed. We further analyze the heating mechanisms in the discharge and the effect of *W* on both plasma kinetics and the deposition rate. rf discharges were also studied and compared to the results from pulsed-dc plasmas.

II. EXPERIMENTAL SETUP

A. Reactor description and operating conditions

A series of DLC films ranging between 200 and 1500 nm thickness was grown by PECVD using either a rf (13.56 MHz) or a pulsed-dc (100 kHz) source in a CH_4 atmosphere. The deposition system included a load-lock chamber and a computer-controlled gas supply.[24] The reactor consisted of a cylindrical vessel of 30 cm diameter and 19.5 cm length, where the cathode (70 cm^2) and the anode (400 cm^2) were placed vertically and 4 cm apart in a capacitive configuration. Monocrystalline silicon wafers were used as substrates. They were placed on the cathode and were kept at room temperature by means of a water cooling circuit. The CH_4 flow was set to 30 SCCM (SCCM denotes cubic centimeter per minute at STP) downstream along the interelectrode gap using a mass flow controller, and it was evacuated with a Roots and a rotary pump. All the processes were carried out at a working pressure *p* of 10 Pa, and a base pressure of 10^{-4} Pa was attained with a turbomolecular pumping system. Film thickness was measured by a Dektak 3030 profilometer.

An asymmetric bipolar pulsed-dc signal was driven to the substrate holder by means of an ENI-RPG-50 power supply operated in power regulation mode. The pulse frequency was fixed at 100 kHz. Figure 1 shows the waveform of the pulsed signal as registered by a high-voltage probe connected to an oscilloscope. The waveform consisted of a fixed positive voltage of around 50 V after an initial overshoot of over 200 V, followed by a variable negative pulse whose peak amplitude ranged between −700 and −1400 V. The signal consisted of two regions, the on and off phases, which

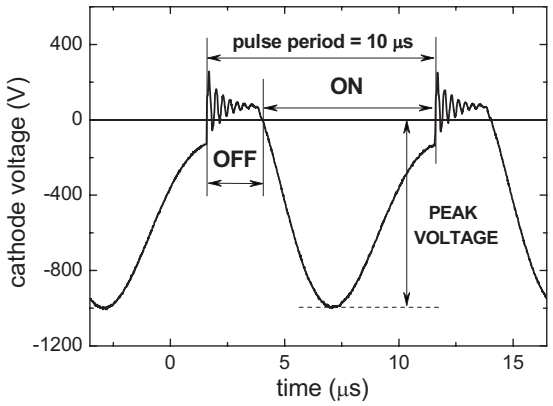

FIG. 1. Asymmetric bipolar pulsed-dc waveform used to excite a CH_4 atmosphere at 10 Pa. The pulse is divided into regions of positive (off) and negative (on) voltages.

correspond to the respective regions of high (negative pulse) and low (positive voltage) *W* input powers. The off phase lasted for 2.096 μs, which defined a duty cycle of 80%. The sum of the on and off times yields the pulse period, which was 10 μs. Deposition was also carried out using a rf signal to power the cathode. For this, a rf power supply was connected to the cathode via a matching network. The power levels led to U_{sb} on the substrate holder of between −200 and −800 V.

B. Data acquisition

A Langmuir probe (SmartProbe, Scientific Systems) was used to determine the *I-V* characteristics of the rf and pulsed-dc discharges. The measuring system consisted of a circuit box connected to a data acquisition card and to an electrostatic probe. The probe consisted of a tungsten wire of 10 mm length with a 0.13 mm radius, which was placed approximately in the middle of the interelectrode gap. It thereby registered the ion and electron currents in the bulk region of the discharge. Each *I-V* scan was the average of many *I-V* sweeps with 1–1000 measurements per point performed in order to increase the signal-to-noise ratio. The plasma parameters (electron temperature T_e, ion density n_i, electron density n_e, floating potential V_f, and V_p) were extracted from each *I-V* curve using the model described in Sec. III.

This system setup was modified in order to monitor the plasma parameters of the pulsed-dc discharges in a time-resolved mode.[36] The internal trigger of the probe box was not synchronized to 100 kHz of the pulsed-dc signal, and the maximal measuring frequency was ~5 kHz. Therefore, the Langmuir probe was connected to a time-delay circuit to perform synchronous measurements of the *I-V* characteristics. As shown in Fig. 2, we used the external trigger entrance to the probe box for this purpose. The light signal supplied by the power source was guided through an optical fiber to a pulse conditioner, which was constituted of a photodiode followed by a signal amplifier together with an analog-digital converter. After this, the signal frequency was reduced by means of a frequency divider, and the resulting signal triggered *I-V* acquisition. The measuring time within

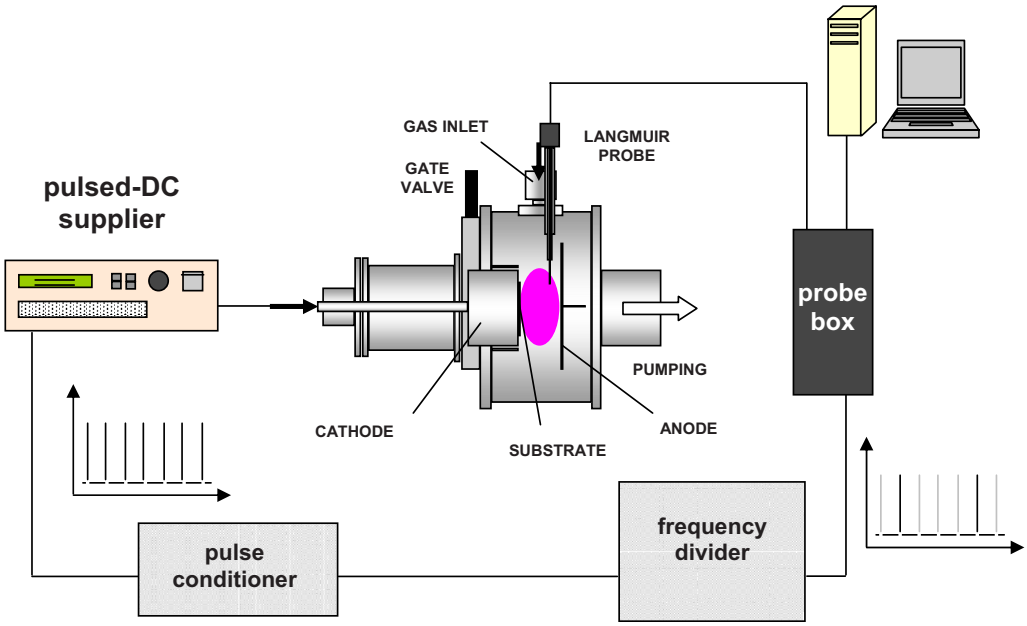

FIG. 2. (Color online) PECVD reactor where the DLC films were grown with a time-delay circuit to operate a Langmuir probe in a time-resolved mode.

the pulse was selected using a pulse generator with a time-delay actuator, which provided a time resolution of 1 μs: ten measurements per pulse.

Since the Langmuir probe was exposed to a CH_4 discharge, it was at risk of becoming progressively coated by a hydrocarbon film which would distort *I-V* acquisition. A cleaning protocol was therefore enacted prior to each measurement. This procedure consisted of biasing the probe to different rf voltages in Ar plasma in order to heat up the probe and to increase the ion bombardment. A discharge in oxygen (O_2) at 0.6 Pa was also systematically carried out to remove contaminants from the chamber walls. Prior to the O_2 treatment, the probe was retracted and protected to prevent oxidation.

III. RESULTS AND DISCUSSION

A. Analysis of the *I-V* characteristics

1. Modeling

The *I-V* curves recorded by the Langmuir probe were modeled to extract the plasma parameters of the rf and pulsed-dc discharges in CH_4. Assuming a nondrifting Maxwellian distribution of electrons, the current collected by the probe i can be modeled as a function of the probe bias V,[44]

$$i = C\sqrt{V_P - V} + i_P \exp\left[\frac{e(V - V_P)}{kT_e}\right], \quad V < V_p, \tag{1}$$

where C is a constant, e is the elementary charge (1.6×10^{-19} C), and κ is Boltzmann's constant (1.38×10^{-23} J/K). The prefactor i_p is the electron current at V_p

$$i_p = n_e eA\left(\frac{\kappa T_e}{2\pi m}\right)^{1/2}, \tag{2}$$

where A is the probe area, and m is the electron mass (9.1×10^{-31} kg). This model is valid up to V_p: the electron saturation region is therefore beyond the range of this model.

The first term of Eq. (1) dominates in the ion saturation region, whereas the second term accounts for the electron current in the retardation zone. The proportionality of the ion current to $\sqrt{V_p - V}$, which agrees well with our measurements, is based on the orbital motion limited (OML) model. The theory of OML according to Langmuir provides acceptable estimations of n_i for weakly ionized (low density, low p) plasmas so long as the sheath is thick compared to the probe radius r_p.[45] According to the criterion used by Chen,[46] discharges fulfilling $r_p/\lambda_D < 3$ may be treated using the OML formalism, where λ_D is the Debye length. This parameter is related to the scale of charge fluctuations in the plasma, thus

$$\lambda_D = \left(\frac{\varepsilon_0 \kappa T_e}{ne^2}\right)^{1/2}, \tag{3}$$

where ε_0 is the permittivity of free space (8.85×10^{-12} F/m) and n is the plasma density. The estimated values of λ_D for rf and pulsed-dc discharges fulfilled the relation with r_p given above, thus justifying the use of OML theory to fit the *I-V* curves.

The average ion mass M_i is dominated by the most abundant ion, which is straightforward in the case of a plasma of an inert element like Ar. However, discharges in hydrocarbon induce many different chemical processes, which produce a large variety of intermediate precursors accompanied by different ionic species. The CH_4 glow discharges studied here are electropositive. According to previous analyses with QMS, CH_4^+, CH_3^+, $C_2H_5^+$, and CH_5^+ are the predominant ions in CH_4 glow discharges:[31,47] they are products of electron impact dissociation and ionization processes. In this work, we assumed that CH_5^+ was the most abundant ion, so the hypothesis $Z=17$ (Z is the atomic number) was considered in our calculations, in contrast to other values proposed in previous works.[36]

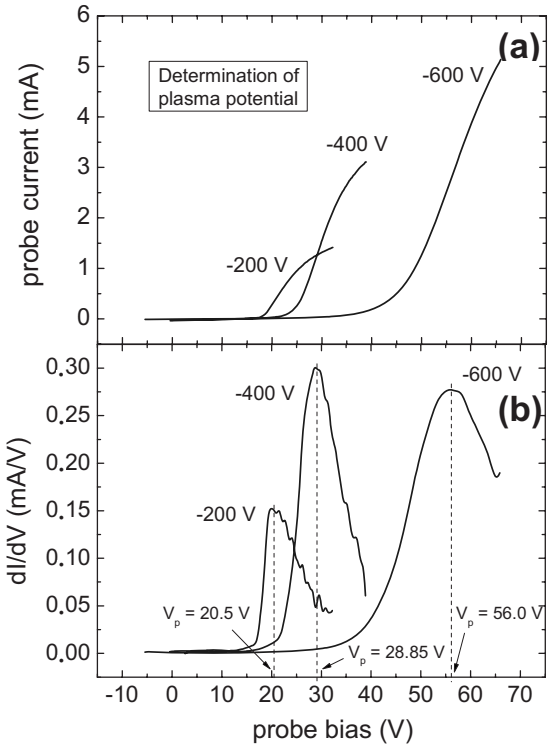

FIG. 3. (a) *I-V* characteristics corresponding to rf discharges in CH_4 powered at different U_{sb} and (b) their first derivatives.

2. Calculation of the plasma parameters

The *I-V* curves were fitted to the above model in order to extract the plasma parameters. The procedure involved the following steps:

(i) Determination of V_p by locating the maximum of the first derivative of *I-V*.
(ii) Plotting the *I-V* curve with current on a logarithmic scale. In this way, the fitting of the ion saturation region is more precise.
(iii) Fitting of Eq. (1) to the logarithmic curve from (ii) above using the least-squares method and optimizing C, n_e, and T_e; a small term I_0 was added to account for small parasitic currents in the probe.
(iv) Estimation of n_i, which must equal to n_e in order to preserve the electric neutrality of the plasma.

B. rf discharges monitored by a Langmuir probe

1. I-V characteristics

The *I-V* curves resulting from rf discharges and their first derivatives corresponding to U_{sb} of −200, −400, and −600 V are plotted in Fig. 3. They show the common features of a Maxwellian distribution of electrons. Namely, Eq. (1) fits the regions of ion saturation and electron retardation. The maximum of the first derivative provided V_p at each U_{sb}.

The −600 V self-bias curve differs considerably from those for −200 and −400 V. The reason of this is explained in the discussion of the plasma parameters below. The *I-V* curves have elevated signal-to-noise ratios, indicative of stable discharges.

2. Plasma parameters

Table I lists the plasma parameters extracted from the *I-V* curves for the rf discharges. Each U_{sb} corresponded to a specific W, which is also given in the table. The succession of columns shows the evolution of the plasma parameters as a consequence of the W variation.

T_e, n_e and V_p increased as U_{sb} increased. At −200 and −400 V of U_{sb}, T_e was of the order of 1 eV, whereas n_e and V_p ranged between $1-5\times10^9$ cm^{-3} and 20–30 V, respectively. At U_{sb} of −600 V, T_e and V_p were much higher. This suggests a substantial change in the discharge dynamics between −400 and −600 V. In fact, the increment step in U_{sb} (200 V) did not correspond to the size of the step in W, which was around 30 W from −200 to −400 V, but more than 50 W to reach −600 V from −400 V. Thus, the plasma parameters responded more linearly to the increase in absorbed power than to the U_{sb} variation. All the parameters were notably higher at a U_{sb} of −600 V, where n_e reached 6.1×10^9 cm^{-3}, indicating four times the degree of ionization at −200 V of self-bias.

The approximation of $Z=17$ was tested using the formula that relates V_p and V_f via T_e

$$V_p - V_f = \frac{kT_e}{2e}\ln\left(\frac{2M_i}{\pi m}\right). \tag{4}$$

T_e was recalculated from this expression and was in agreement with the values in Table I to within 0.5 eV. Although the sensitivity of Eq. (4) to M_i is poor, this result supports the selection of CH_5^+ as the most abundant ion.

In the OML theory, the prefactor C in Eq. (1) is proportional to n_i. Despite the relatively good fit of our *I-V* curves to Eq. (1), the values of n_i are normally overestimated. Ignoring distortions introduced by rf powering,[48] this excess in n_i is a consequence of the charge exchange collisions produced in the probe sheath.[49] Therefore, n was identified with n_e. More sophisticated models of the ion current that correct such overestimation due to collisions have been applied to the diagnostics of high-density plasmas ($n \geq 10^{11}$ cm^{-3}).[46,50]

TABLE I. Variation in plasma parameters for rf source in CH_4 as a function of U_{sb} and W. We have assumed $n \approx n_e$.

U_{sb} (V)	W (W)	T_e (eV)	n (10^9 cm^{-3})	V_p (V)	V_f (V)
−200	13	1.0	1.5	21	18
−400	43	1.9	4.7	29	23
−600	100	5.3	6.1	56	34

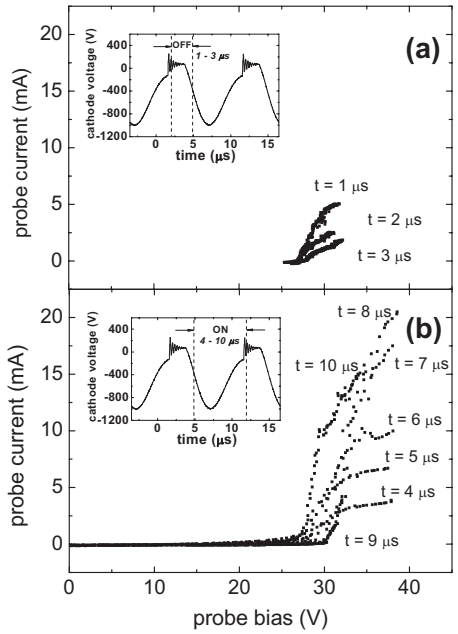

FIG. 4. *I-V* curves for a pulsed-dc discharge in CH_4 with a peak voltage of −900 V recorded during the (a) off and (b) on phases. The insets show the part analyzed within the pulse cycle.

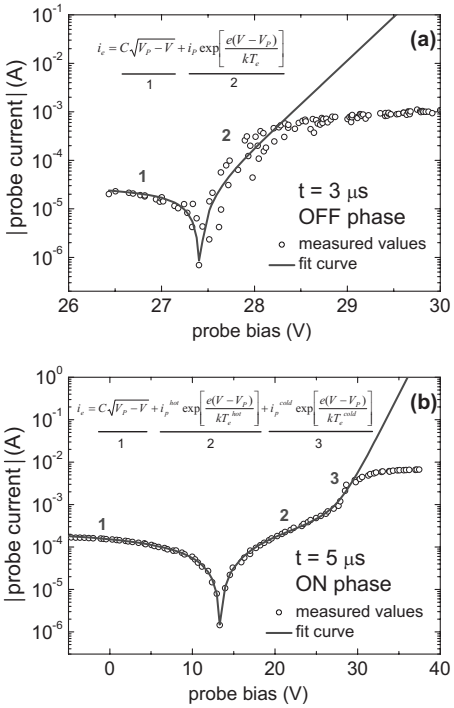

FIG. 5. Respective fittings of Eqs. (1) and (5) to *I-V* curves registered during the (a) off and (b) on phases of a pulsed-dc discharge. The absolute values of current are plotted on a log scale.

C. Bipolar pulsed-dc discharges monitored by a fast Langmuir probe

1. Time-resolved recording of I-V characteristics

Figure 4 shows the evolution with a time step of 1 μs of *I-V* curves corresponding to pulsed-dc discharges in CH_4 excited by a peak voltage of −900 V. The curves from the off phase are displayed in Fig. 4(a). They show a progressive weakening of the probe signal due to the low positive bias of the electrode. These measurements show a low signal-to-noise ratio, which is evidence of a very weak discharge. The signals measured during the on phase were more intense [Fig. 4(b)]. Their shapes reveal the non-Maxwellian nature of the plasma.

Each characteristic was fitted to the *I-V* model described above to obtain the plasma parameters (Fig. 5). The curves for the off region fit the model for Maxwellian electrons [Eq. (2)]. Despite the low intensity of the signal (which made fitting difficult), the plasma parameters indicated active discharge. This is confirmed by the smooth variation of V_p during the pulse, as discussed below. However, the on phase yielded *I-V* curves that could not be fitted to the model above. Instead, they were successfully fitted to a two-temperature model. To do this, Eq. (1) was generalized to the following [which accounts for the presence of two electron populations (cold and hot) in the on phase]:

$$i = C\sqrt{V_P - V} + i_p^{\text{hot}} \exp\left[\frac{e(V - V_P)}{kT_e^{\text{hot}}}\right] + i_p^{\text{cold}} \exp\left[\frac{e(V - V_P)}{kT_e^{\text{cold}}}\right], \quad V < V_p. \tag{5}$$

Here, the intensities at V_p have the same dependences as in Eq. (2),

$$i_p^{\text{hot}} = n_e^{\text{hot}} eA\left(\frac{kT_e^{\text{hot}}}{2\pi m}\right)^{1/2}, \tag{6}$$

$$i_p^{\text{cold}} = n_e^{\text{cold}} eA\left(\frac{kT_e^{\text{cold}}}{2\pi m}\right)^{1/2}. \tag{7}$$

Then, n_e is calculated as

$$n_e = n_e^{\text{hot}} + n_e^{\text{cold}}. \tag{8}$$

Figure 5, which is plotted against a logarithmic scale, shows the Maxwellian electron distribution in the off phase, which switches to a bi-Maxwellian distribution as soon as the on phase of the pulse started. Naturally, these two groups of electrons merge again into a single population at the start of the next off phase.

Two-temperature electron populations are typically found in weakly ionized plasmas at low p and indicate that the electron energy distribution function departs from thermodynamic equilibrium. Sheridan *et al.*[51] reported them for dc discharges in helium and Godyak *et al.*[52] analyzed different non-Maxwellian plasmas with probe diagnostics. In the field of pulsed plasmas, Bäcker and Bradley[37] thoroughly investigated the effects of incorporating magnetrons into the plasma parameters, such as, for instance, the generation of bi-Maxwellian discharges induced by the presence of a magnetic field.

2. Tracking plasma parameters

a. Electron temperature Figure 6 shows the evolution of T_e within pulses with a peak voltage of −700, −900, and −1100 V. The behavior of this variable was clearly differentiated between the regions of the pulse. During the off phase,

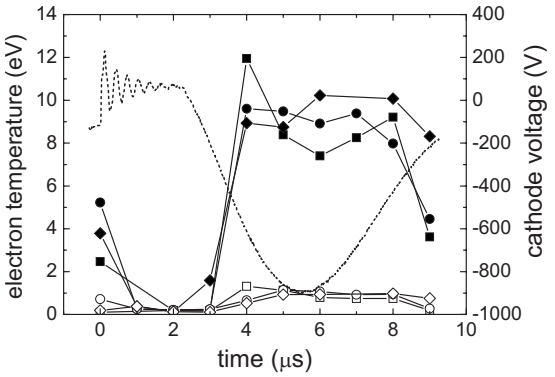

FIG. 6. Evolution of T_e^{cold} and T_e^{hot} together with the pulse waveform (dotted line). Solid symbols correspond to the hot population and outlines correspond to the cold group. Squares: −700 V; circles: −900 V; rhombuses: −1100 V.

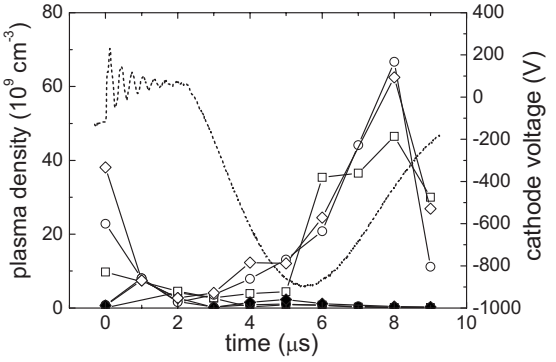

FIG. 7. Evolution of n_e^{hot} and n_e^{cold} together with the pulse waveform (dotted line). Solid symbols correspond to the hot electrons and outlines correspond to the cold electrons. Squares: −700 V; circles: −900 V; rhombuses: −1100 V.

there was a single group of electrons with a T_e of less than 1 eV. This was followed by the generation of a hot population of electrons within the initial 2 μs of the on phase. The hot electrons had temperatures of over 10 eV, which then fell during this phase, whereas the cold group reached a plateau of the order of 1 eV. Bradley *et al.*[53] observed a hot burst of electrons confined by means of a magnetron in plasma subjected to 100 kHz dc pulses. Their T_e peaked at transition between the on and off phases.

The splitting into two of the electron population of the pulsed-dc plasma might be the result of an additional heating mechanism that is activated during the on phase. The literature reports that the oscillating sheath edge at the cathode is a relevant source of hot electrons.[46] Such excitation is known as stochastic heating and it selectively excites high-energy electrons at low p, while low-energy electrons remain cold. The selectivity of such energy transfer is the key to the electrons forming a bi-Maxwellian population. The on time may have been too short to avoid this burst of hot electrons cooling down and merging with the cold population. This hypothesis of thermalization should be verified by long-term analysis of the temperature decay within a pulse.

Bäcker and Bradley[37] supposed that secondary electrons from the cathode were firmly pushed into the bulk of the plasma by the contracting sheath, leading to an increase in T_e. Using Langmuir probe diagnostics, Glocker showed that ac discharges resulted in electrons that were more energetic than in dc-powered plasmas. This was attributed to the rapidly advancing sheath edge at the beginning of the on phase when a burst of hot electrons coming from the sheath was injected into the plasma.[54] This effect may be further explained by considering the ionic speed of sound (Bohm velocity) u_i,[55]

$$u_i = \left(\frac{\kappa T_e}{M_i}\right)^{1/2}. \tag{9}$$

According to the values of T_e and n_e at the off-on transition, u_i was lower than 2000 m/s, whereas the sheath-edge velocity was more than 10^4 m/s. This velocity was estimated from the temporal variation in the collisional sheath thickness s,[44]

$$s = \left[\frac{4.12}{\pi}\left(\frac{eV_0}{\kappa T_e}\right)^3 \lambda_i \lambda_{Ds}^4\right]^{1/5}, \tag{10}$$

where λ_i is the mean free path of the ions and λ_{Ds} is the Debye length at the sheath edge. According to Peter *et al.*,[42] the value of λ_i for CH_4 at a p of 10 Pa is around 1.2 mm, which is of the order of or lower than s. The value of n at the sheath edge is assumed to be $n_s \approx 0.63 n_e$. In this case, V_0 equals V_p minus the cathode voltage.

Since the sheath edge moved faster than the ionic sound within the first microsecond of the on phase, instabilities generated by energetic acoustic waves could be associated with the burst of hot electrons. This could be the key to achieving high n in pulsed-dc discharges, as explained below. This hypothesis, based on the rapid motion of ions, cannot be used for rf discharges, in which the ions constantly flow toward the reactor walls since they cannot follow the oscillations of the electric field. This, together with the fact that collisionless heating becomes inefficient at higher frequencies,[56] might explain why the rf discharges in CH_4 did not result in bi-Maxwellian distributions.

b. Plasma density n_e was evaluated every 1 μs from the probe current at V_p, and its behavior during the pulse is plotted in Fig. 7. It oscillated between 2×10^9 and 8×10^9 cm^{-3} in the off region. As opposed to T_e, n_e^{cold} gradually increased once the on phase started and peaked at ~2.5 μs after the peak voltage. Similar patterns were observed by Lieberman and Ashida[57] and Richter *et al.*[38] This delay in reaching the maximum can be attributed to the relatively high inertia of ions reacting to perturbations of the electric field, compared to the fast response of the electrons. The response time of each species is limited by its respective plasma frequency. After the peak, n_e^{cold} fell sharply, coinciding with the positive voltage region.

The discharges at −900 and −1100 V produced an exponential evolution in n_e^{cold} until it reached its maximal value, which surpassed 6×10^{10} cm^{-3}: 10 times higher than in the case of the rf signal. A smaller increase was measured for less energetic pulses (−700 V), where n_e^{cold} approached 5×10^{10} cm^{-3}. The hot electrons had a relatively low density all the time: generally below 10^9 cm^{-3}. This may represent the reduced fraction of hot electrons boosted by the sheath edge when the on phase started. As the pulse continued, the

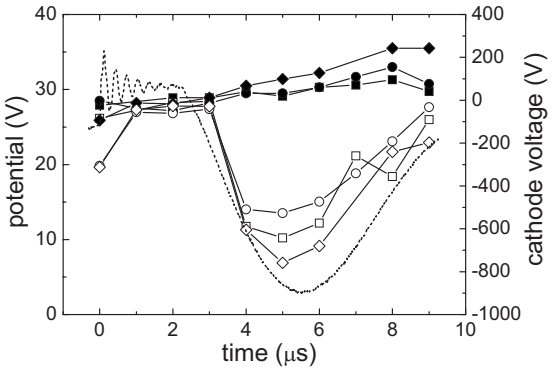

FIG. 8. Evolution of V_p and V_f together with the pulse waveform (dotted line). Solid symbols correspond to V_p and outlines correspond to V_f. Squares: −700 V; circles: −900 V; rhombuses: −1100 V.

cold population increased, corresponding to a decrease in n_e^{hot} and in T_e^{hot}. This indicates the cooling down of the hot group, whose energy was partly spent enhancing the ionization.

Due to the strong oscillations of the probe sheath associated with pulsed plasmas, time-resolved measurements of n_i were not reliable.[58] This is especially true for the off phase when the probe sheath expands so much that n_i is overestimated according to Ref. 45. The low signal-to-noise ratio of the recorded *I-V* curves was another problem during the off phase. Therefore, the corresponding data points were not considered. However, the velocity of the ion response to voltage changes was limited by the ion plasma frequency, as indicated above. Electrons are the best tracers of fast transitions in the driving voltage and V_p. The value of n is therefore more accurately monitored by considering n_e, not n_i calculated for the ion saturation region.

c. Plasma and floating potentials Figure 8 shows the evolution of V_p and V_f during the pulse. V_p, which ranged from 25 to 35 V, showed a monotonic and smooth increase during the whole period. It only decreased sharply at the transition from on to off when the polarity of the electrode was inverted. The fact that V_p did not vanish during the off phase indicates that the discharge was never completely extinguished. This is an important point with regard to plasma stability, the minimization of arcs, and maintaining the deposition rate. Since V_p was stable during the off phase, we can infer that the decay time of the plasma was longer than 2 μs. This is related to the time scale of charge redistribution and recombination in the positive voltage region, which is limited by the ion motion.

V_f evolved parallel to the cathode voltage: its behavior was connected to the variation in T_e according to Eq. (5). From this expression an "effective" T_e can be derived, whose value is between T_e^{hot} and T_e^{cold}.

3. Averaged parameters

Table II gives the plasma parameters averaged over one period for different peak voltages. T_e^{hot} and T_e^{cold} show no definite trend with respect to W. Increasing W did influence n_e, although variation was small. The same applies to V_p and V_f. In contrast to the U_{sb} resulting from rf discharges, the variation in the peak voltage in pulsed-dc CH_4 discharges did not produce major changes in the plasma parameters. Thus, the peak voltage as well as W can be used as external parameters to control the ion energy without drastically changing the discharge structure.

n was treated as the estimated value of n_e. As noted above, evaluations of n from the ion saturation region in pulsed plasmas are imprecise and lead to important deviations from electrical neutrality.

It is worth noting that the average n surpassed 2×10^{10} cm^{-3}, which correspond to ionization rates between three and four times higher than for rf discharges. Therefore, pulsed-dc power not only provided large ion energies through high peak voltages, but it also gave rise to more active plasmas, thanks to stronger ionizations than those produced by the rf source. This could explain the significant increase in DLC deposition rates obtained using pulsed-dc compared to rf PECVD, as reported by Andújar *et al.*[24] However, DLC deposition is associated with the on phase, where the plasma becomes more active. During the off phase, ionization was weaker as indicated by the lower values of T_e and n_e. This leads to a reduction in compressive stress due to the accommodation of the deposited species at more stable sites.[24]

D. Input power and deposition rate

1. Growth regimes

We analyzed the growth of the DLC films through the technical parameters of deposition. We studied the dependence of the deposition rate on W into the CH_4 discharge. W per unit gas flow W/F is a parameter that is useful for studying the dynamics of PECVD from hydrocarbon precursors.[14,59] W/F can be interpreted as the rate of energy imparted per particle, and it is related to the mass deposition rate R_m through the following expression, which is valid for radical-dominated plasma processes at moderate energies:[60,61]

$$\frac{R_m}{F} = G \exp\left(-\frac{E_a}{W/F}\right), \tag{11}$$

where F is the gas flow and G is a reactor-dependent factor. The parameter E_a is a characteristic of the gas used, and it is

TABLE II. Plasma parameters averaged over one pulse for 100 kHz pulsed-dc discharges in CH_4 at different W. We have assumed $n \approx n_e^{\text{cold}} + n_e^{\text{hot}}$.

Peak voltage (V)	W (W)	T_e^{hot} (eV)	T_e^{cold} (eV)	n_e^{hot} (10^9 cm^{-3})	n_e^{cold} (10^9 cm^{-3})	n (10^9 cm^{-3})	V_p (V)	V_f (V)
−700	18	5.7	0.60	1.0	19	20	30	20
−900	34	5.6	0.64	1.4	20	21	30	21
−1100	52	5.8	0.55	1.9	21	23	31	19

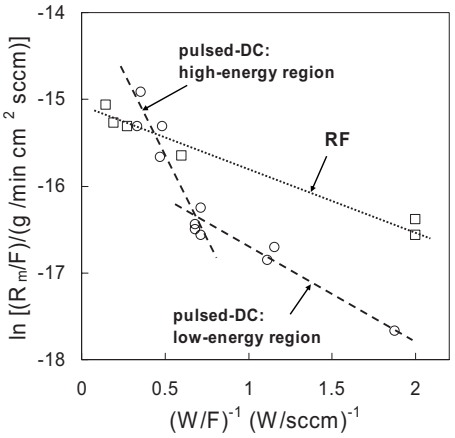

FIG. 9. Arrhenius-type plots that relate R_m to W for DLC samples deposited by rf and pulsed-dc discharges in CH_4.

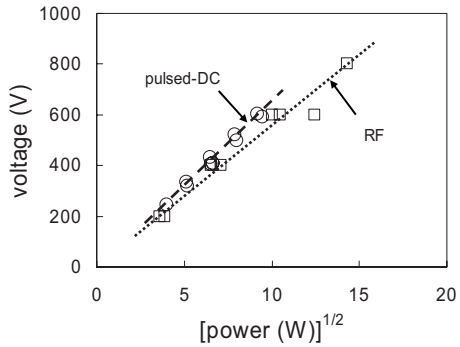

FIG. 10. Variation in the cathode voltage with W for rf- and pulsed-DC PECVD processes.

defined as the energy required to yielding significant fragmentation and polymerization of the precursor. The factor G is proportional to the maximal x_{dep} of the precursor gas to deposited film, which indicates the deposition efficiency[62]

$$x_{dep} = GA_{dep}\frac{RT_0}{M_p p_0}. \tag{12}$$

In this formula, A_{dep} is the deposition area, R is the ideal gas constant (8.31 J K^{-1} mol^{-1}), M_p is the molecular mass of the precursor, and T_0 and p_0 are the respective temperature and pressure under standard conditions. The average density of DLC is considered to be 1.9 g/cm^3.[36] Equation (11) requires that the residence time of gas species τ is much longer than the pulse period.[30] This condition is fulfilled since τ is 2.8 s. Hegemann *et al.*[61,62] used this formalism to study polymer depositions by PECVD. Bauer *et al.*[63] considered the average energy dissipated per gas molecule in a pulsed discharge, a parameter similar to W/F, which permitted the control of the plasma chemistry.

Figure 9 shows the Arrhenius-type plots of R_m/F as a function of $(W/F)^{-1}$ for DLC depositions and Table III lists the parameters fitted from Eq. (11). The range of W/F analyzed is within the optimal interval for film deposition from CH_4 plasma, as reported in Ref. 28. The data points for the rf processes are linear. E_a and G were extracted from the linear fit analysis of these data using Eq. (11). A value of 41.4 J/cm^3 was obtained for E_a, in agreement with that reported by Hegemann[64] for an asymmetric rf discharge in CH_4. The low x_{dep} of only 2.9% indicates a process with poor conversion of the precursor. In the plot of growth processes using pulsed-dc energy, two regions with different E_a were detected. The value of W/F corresponding to a peak voltage of −1000 V marked the limit between low- and high-energy processes.

TABLE III. Parameters from Eqs. (11) and (12) for the PECVD of DLC films grown with rf and pulsed-dc energy.

	E_a (J cm^{-3})	G ($\times 10^{-7}$ g min^{-1} cm^{-2} $SCCM^{-1}$)	X_{dep} (%)
rf	41.4	2.8	2.9
Pulsed-dc (low E)	60.6	1.5	1.6
Pulsed-dc (high E)	228	10	11

The low-energy region is located on the right of the Arrhenius-type plot. It is associated with a set of growth mechanisms, which are characterized by an E_a of 60.6 J/cm^3 and an x_{dep} of 1.6%. As W increased, the system crossed the energy threshold and entered the high-energy region. There, a second set of growth mechanisms dominated DLC deposition. This regime was more efficient than that which was dominant at low energies with x_{dep} reaching 11%. Moreover, E_a increased by a factor of 4, indicating that the deposition process involved increased decomposition of the CH_4 molecules at high electric fields. E_a is connected to the bond breakage energy of the precursor molecule.[61] Therefore, the change in E_a accounts for the activation of new intermediate precursors responsible for film deposition. Finally, rf and low-energy pulsed-dc discharges of CH_4 presented similar values of E_a. This suggests comparable plasma chemistry and kinetics in the two types of excitation.

2. Power dissipation modes

The heating mechanism dominant in a glow discharge depends strongly on p. According to Lieberman and Lichtenberg,[44] our discharges were cold plasmas developed between intermediate- and high-p regimes because $\lambda_i/d \approx T_i/T_e$, where d is the interelectrode distance. The ion temperature T_i was close to room temperature. The dominant heating mechanism for rf discharges in CH_4 at this p was observed by Peter *et al.*[42] to be Ohmic heating. Processes heated by such a mechanism fulfill

$$\frac{-U_{sb}}{W^{1/2}} = A - Bp, \tag{13}$$

where A and B are empirical constants. Figure 10 shows that our rf discharges followed an Ohmic regime since $U_{sb} \sim W^{1/2}$. Pulsed-dc plasmas were also analyzed using this formalism, where U_{sb} was substituted by the average pulse voltage. From Fig. 10 one could infer that Ohmic heating was also dominant for the pulsed-dc discharges, although stochastic heating played an important role at the pulse time scales, as discussed in Sec. III C 2.

Figure 10 suggests that the associated resistance of the pulsed-dc plasma was independent of W, despite the changes

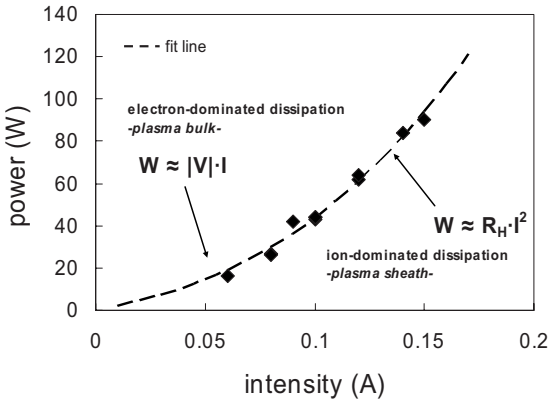

FIG. 11. Evolution of W with I measured for pulsed-dc plasmas in CH_4.

in the growth regime and E_a observed in Fig. 9. The analysis of the power dissipation mode in the discharge may shed some light on this issue. It is accepted that the power share in rf discharges depends on the driving intensity I according to[65]

$$W_{\text{total}} = W_{\text{bulk}} + W_{\text{sheath}} = |V|I + R_{\text{sh}}I^2, \tag{14}$$

where W_{total} is the total power absorbed by the plasma, W_{bulk} and W_{sheath} are the power consumed by the bulk of the plasma and the sheath, respectively, $|V|$ is an effective plasma potential, and R_{sh} is the sheath resistance: $R_{\text{sh}} \sim I^{0.5}$. Many experimental studies also confirm the dependence of R_{sh} on the frequency and pressure.[66–68] At low W, the energy is preferably deposited in the plasma bulk, but as W increases the dissipation zone is displaced to the sheath. Figure 11 shows this evolution for pulsed-dc discharges.

Figure 12 maps the evolution of the power share as a function of the parameter W/F by fitting Eq. (14) to the data from pulsed-dc CH_4 discharges. The relation $W_{\text{sheath}}/W_{\text{total}}$ evolves parallel to R_m/F versus $(W/F)^{-1}$ displayed in Fig. 9. Moreover, the transition of the power dissipation mode coincides with the threshold power for the transition of growth regimes.

The depositions performed in the low-energy region (on the right in Fig. 9) corresponded to processes in which power dissipation was bulk dominated. There, the energy supplied was mainly consumed by the electrons populating the bulk.

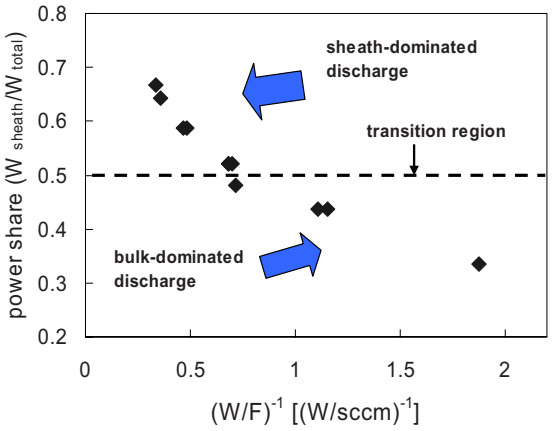

FIG. 12. (Color online) Power share in plasma volume as a function of $(W/F)^{-1}$.

However, the high-energy processes (on the left in Fig. 9) were sheath dominated, i.e., the ions in the plasma sheath absorbed the highest fraction of W. First, we can conclude that low-energy pulsed-dc discharges provoked a little dissociation of the CH_4 molecules and the majority of W was transferred to the chemical processes taking place in the bulk of the plasma. This poor decomposition of CH_4 is reflected by the relatively low E_a. Second, the high-energy processes were characterized by an increased degree of dissociation of the precursor, which corresponds to a displacement of power dissipation to the sheath. This could be explained by energy saturation of the electrons in the plasma bulk. The excess energy is then utilized to accelerate the ions in the sheath toward the cathode and to enhance the stochastic heating of the electrons.

IV. CONCLUSIONS

The study of bipolar pulsed-dc CH_4 discharges to deposit DLC films was successfully performed by means of plasma diagnostics with a fast Langmuir probe. The time-resolved monitoring of the plasma parameters showed many peculiarities of this type of plasmas, as compared to rf discharges. Dividing the pulses into on and off phases provided a practical way to discuss parameter evolution within a cycle. From this analysis, we observed that the pulsed-dc discharges did not bring about a stationary state. The almost constant V_p was indicative of a never-vanishing discharge. T_e and n_e showed relatively low values during the off phase. Electrons at two different temperatures were detected during the on phase, probably due to stochastic heating from the rapidly advancing sheath edge during the polarity reversal. Values of around 10 eV were measured for the hot electrons, which had a low-density population. The cold electrons, which reached almost 7×10^{10} cm^{-3} at the end of the on phase, constituted the majority population. The temporal evolution of the plasma parameters, together with the energetic ions generated by the peak voltage, was advantageous for the growth of DLC films with improved mechanical properties. Moreover, the plasma parameters showed a relatively smooth response to the variation in the peak voltage. Other distinctive points of pulsed-dc plasmas were the two different growth regimes, as determined by the parameter W/F, due to the variation in E_a. The high-energy depositions had higher x_{dep} and caused more dissociations of the precursor molecules. This behavior was connected to a transition from bulk- to sheath-dominated power dissipation. Table IV summarizes the results of the comparative study.

This work has shown fundamental strengths of using pulsed-dc plasmas to deposit DLC films from CH_4 atmospheres. A more complete study requires the exploration of the remaining pulse variables (duty cycle, frequency, etc.) as well as the evaluation of the plasma parameters in space-resolved mode and with alternative techniques.

ACKNOWLEDGMENTS

This research was partially supported by the projects MAT2003-02997 and DPI2007-61349 of the Spanish Ministry of Education and Science. C.C. and M.R. acknowledge

TABLE IV. Main characteristics of rf and pulsed-dc discharges in CH_4 used to grow DLC films.

rf (13.56 MHz)	Pulsed-dc (100 kHz)
One input parameter (U_{sb})	Tailoring of signal (peak voltage, duty cycle, positive voltage)
Discharge in steady state	Succession of transient states
Maximal ion energy around 500 eV	Peak voltage up to −1400 V
Plasma parameters very sensitive to U_{sb}	Smooth variation in plasma parameters with peak voltage
One T_e (Maxwellian population)	T_e^{hot} and T_e^{cold}(bi-Maxwellian population)
10^{-5} degree of ionization at −600 V self-bias	Peak in degree of ionization ten times higher than for rf
Low x_{dep}	Greater deposition efficiency
Plasma processes described by a constant E_a	Two growth regimes indicated by a variation in E_a
Ohmic heating	Ohmic+stochastic heating

the financial support from the Spanish Ministry of Science and Innovation (Juan de la Cierva contract) and from the Spanish Research Council (Grant No. UAC-2005-0021), respectively.

[1]T. Lampe, S. Eisenberg, and E. Rodríguez Cabeo, Surf. Coat. Technol. **174-175**, 1 (2003).
[2]R. Hauert and J. Patscheider, Adv. Eng. Mater. **2**, 247 (2000).
[3]M. Ohring, *The Materials Science of Thin Films* (Academic, New York, 2002).
[4]J. R. Roth, *Industrial Plasma Engineering* (Institute of Physics, University of Reading, Berkshire, 2001), Vol. 2.
[5]R. A. Scholl, Surf. Coat. Technol. **98**, 823 (1998).
[6]J. Laimer, M. Fink, T. A. Beer, and H. Störi, Surf. Coat. Technol. **174-175**, 118 (2003).
[7]A. Lacoste and J. Pelletier, in *Plasma Polymers and Related Materials*, edited by M. Mutlu, G. Dinescu, R. Förch, J. M. Martín-Martínez, and J. Vyscocyl (Hacettepe University Press, Ankara, 2005), p. 1.
[8]M. Liehr, S. Wieder, and M. Dieguez-Campo, Thin Solid Films **502**, 9 (2006).
[9]H. Yasuda, *Luminous Chemical Vapor Deposition and Interface Engineering* (Marcel Dekker, New York, 2005).
[10]H.-U. Poll and S. Schreiter, Surf. Coat. Technol. **93**, 105 (1997).
[11]J. Schmitt, M. Elyaakoubi, and L. Sansonnens, Plasma Sources Sci. Technol. **11**, A206 (2002).
[12]J. Perrin, J. Schmitt, C. Hollenstein, A. Howling, and L. Sansonnens, Plasma Phys. Controlled Fusion **42**, B353 (2000).
[13]N. Kaiser and H. K. Pulker, *Optical Interference Coatings* (Springer, Berlin, 2003).
[14]C. Corbella, I. Bialuch, M. Kleinschmidt, and K. Bewilogua, Solid State Sci., in press (2009).
[15]S. Röhlecke, R. Tews, A. Kottwitz, and K. Schade, Surf. Coat. Technol. **74-75**, 259 (1995).
[16]E. H. A. Dekempeneer, L. Poirier, J. P. Lebrun, A. Pasgrimaud, Y. Desalos, and F. Balanck, Surf. Coat. Technol. **151-152**, 462 (2002).
[17]T. Michler, M. Grischke, I. Traus, K. Bewilogua, and H. Dimigen, Diamond Relat. Mater. **7**, 459 (1998).
[18]A. Anders, Surf. Coat. Technol. **200**, 1893 (2005).
[19]C. Corbella, I. Bialuch, M. Kleinschmidt, and K. Bewilogua, Thin Solid Films **517**, 1125 (2008).
[20]S. Aisenberg and R. Chabot, J. Appl. Phys. **42**, 2953 (1971).
[21]J. Robertson, Mater. Sci. Eng. R. **37**, 129 (2002).
[22]R. Hauert, Tribol. Int. **37**, 991 (2004).
[23]C. Donnet and A. Erdemir, *Tribology of Diamond-Like Carbon Films. Fundamentals and Applications* (Springer, New York, 2008).
[24]J. L. Andújar, M. Vives, C. Corbella, and E. Bertran, Diamond Relat. Mater. **12**, 98 (2003).
[25]A. von Keudell, M. Meier, and C. Hopf, Diamond Relat. Mater. **11**, 969 (2002).
[26]C. Corbella, B. Echebarría, L. Ramírez-Piscina, E. Pascual, J. L. Andújar, and E. Bertran, Appl. Phys. Lett. **87**, 213117 (2005).
[27]M. Rubio-Roy, C. Corbella, J. García-Céspedes, M. C. Polo, E. Pascual, J. L. Andújar, and E. Bertran, Diamond Relat. Mater. **16**, 1286 (2007).
[28]A. Pastol and Y. Catherine, J. Phys. D **23**, 799 (1990).
[29]T. Wallendorf, S. Marke, and R. Bandorf, 49th SVC Annual Technical Conference Proceedings, 2006 (unpublished), p. 413.
[30]M. Bauer, T. Schwarz-Selinger, W. Jacob, and A. von Keudell, J. Appl. Phys. **98**, 073302 (2005).
[31]H. Sugai and H. Toyoda, J. Vac. Sci. Technol. A **10**, 1193 (1992).
[32]D. Gahan, B. Dolinaj, and M. B. Hopkins, Rev. Sci. Instrum. **79**, 033502 (2008).
[33]N. Hershkowitz, in *Plasma Diagnostics*, edited by O. Auciello and D. L. Flamm (Academic, New York, 1989), Vol. 1, p. 113.
[34]V. I. Demidov, S. V. Ratynskaia, and K. Rypdal, Rev. Sci. Instrum. **73**, 3409 (2002).
[35]D. Gahan, B. Dolinaj, and M. B. Hopkins, Plasma Sources Sci. Technol. **17**, 035026 (2008).
[36]C. Corbella, M. C. Polo, G. Oncins, E. Pascual, J. L. Andújar, and E. Bertran, Thin Solid Films **482**, 172 (2005).
[37]H. Bäcker and J. W. Bradley, Plasma Sources Sci. Technol. **14**, 419 (2005).
[38]F. Richter, Th. Welzel, Th. Dunger, and H. Kupfer, Surf. Coat. Technol. **188-189**, 384 (2004).
[39]A. Hallil and B. Despax, Thin Solid Films **358**, 30 (2000).
[40]A. Joshi, S. A. Gangal, and S. K. Kulkarni, J. Appl. Phys. **64**, 6668 (1988).
[41]R. G. Lacerda, V. Stolojan, D. C. Cox, S. R. P. Silva, and F. C. Marques, Diamond Relat. Mater. **11**, 980 (2002).
[42]S. Peter, K. Graupner, D. Grambole, and F. Richter, J. Appl. Phys. **102**, 053304 (2007).
[43]A. L. Alexandrov and I. V. Schweigert, Plasma Sources Sci. Technol. **14**, 209 (2005).
[44]M. A. Lieberman and A. J. Lichtenberg, *Principles of Plasma Discharges and Materials Processing* (Wiley, New York, 2005).
[45]F. F. Chen, in *Plasma Diagnostic Techniques*, edited by R. H. Huddlestone and S. L. Leonard (Academic, New York, 1965), p. 113.
[46]F. F. Chen, Phys. Plasmas **8**, 3029 (2001).
[47]H. Toyoda, H. Kojima, and H. Sugai, Appl. Phys. Lett. **54**, 1507 (1989).
[48]M. Tuszewski and J. A. Tobin, Plasma Sources Sci. Technol. **5**, 640 (1996).
[49]Z. Sternovsky, S. Robertson, and M. Lampe, Phys. Plasmas **10**, 300 (2003).
[50]A. Karamcheti and Ch. Steinbrüchel, J. Vac. Sci. Technol. A **17**, 3051 (1999).
[51]T. E. Sheridan, M. J. Goeckner, and J. Goree, J. Vac. Sci. Technol. A **9**, 688 (1991).
[52]V. A. Godyak, R. B. Piejak, and B. M. Alexandrovich, J. Appl. Phys. **73**, 3657 (1993).
[53]J. W. Bradley, H. Bäcker, P. J. Kelly, and R. D. Arnell, Surf. Coat. Technol. **142–144**, 337 (2001).
[54]D. A. Glocker, J. Vac. Sci. Technol. A **11**, 2989 (1993).
[55]A. Fridman and L. A. Kennedy, *Plasma Physics and Engineering* (Taylor & Francis, New York, 2004).
[56]S. J. You, S. K. Ahn, and H. Y. Chang, Appl. Phys. Lett. **89**, 171502 (2006).
[57]M. A. Lieberman and S. Ashida, Plasma Sources Sci. Technol. **5**, 145 (1996).
[58]X. Tang and D. M. Manos, Plasma Sources Sci. Technol. **8**, 594 (1999).
[59]H. Yasuda and T. Hirotsu, J. Polym. Sci., Polym. Chem. Ed. **16**, 743 (1978).
[60]Y. S. Yeh, I. N. Shyy, and H. Yasuda, J. Appl. Polym. Sci.: Appl. Polym. Symp. **42**, 1 (1988).
[61]D. Hegemann, M. M. Hossain, E. Körner, and D. J. Balazs, Plasma Processes Polym. **4**, 229 (2007).

[62]D. Hegemann, C. Oehr, and A. Fischer, J. Vac. Sci. Technol. A **23**, 5 (2005).
[63]M. Bauer, T. Schwarz-Selinger, H. Kang, and A. von Keudell, Plasma Sources Sci. Technol. **14**, 543 (2005).
[64]D. Hegemann, Thin Solid Films **515**, 2173 (2006).
[65]C. Beneking, J. Appl. Phys. **68**, 4461 (1990).
[66]V. A. Godyak, R. B. Piejak, and B. M. Alexandrovich, IEEE Trans. Plasma Sci. **19**, 660 (1991).
[67]S. J. You, H. C. Kim, C. W. Chung, H. Y. Chang, and J. K. Lee, J. Appl. Phys. **94**, 7422 (2003).
[68]S. J. You, S. K. Ahn, and H. Y. Chang, Surf. Coat. Technol. **193**, 81 (2005).